2021 43rd Annual International Conference of the
IEEE Engineering in Medicine & Biology Society (EMBC)
Oct 31 - Nov 4, 2021. Virtual Conference

Pixel Intensity Vector Field: An Inside Out Approach of Looking at Ultrasound Reflections from the Lung at High Frame Rates

Gayathri Malamal, *Student Member, IEEE* and Mahesh Raveendranatha Panicker, *Senior Member, IEEE*

***Abstract*— Ultrasound (US) imaging is becoming the routine modality for the diagnosis and prognosis of lung pathologies. Lung US imaging relies on artifacts from acoustic impedance (Z) mismatches to distinguish and interpret the normal and pathological lung conditions. The air-pleura interface of the normal lung displays specularity due to the huge Z mismatches. However, in the presence of pathologies, the interface alters exhibiting a diffuse behavior due to increased density and reduced spatial distribution of air in the sub-pleural space. The specular or the diffuse behavior influences the reflected acoustic intensity distribution. This study aims to understand the reflection pattern in a normal and pathological lung through a novel approach of determining pixel-level acoustic intensity vector field (IVF) at high frame rates. Detailed lung modeling procedures using k-Wave US toolbox under normal, edematous, and consolidated conditions are illustrated. The analysis of the IVF maps on the three lung models clearly shows the drifting of the air-pleura interface from specular to diffuse with the severity of the pathology.**

***Clinical Relevance*— The presented acoustic simulation lung models are an aid to teaching and research by providing a quick visual and intuitive understanding of lung ultrasound physics. The proposed intensity vector field maps are supplementary information to aid diagnostics and characterization of any tissue composed of specular and diffuse components.**

I. Introduction

Ultrasound (US) imaging has been gaining increased traction in recent times as the main clinical imaging modality for lung diagnostics and progression monitoring compared to chest radiography and computed tomography. This is attributed to the portability, simplicity, dynamicity, relative inexpensiveness, and absence of ionizing radiations offered by lung US that facilitates its use at the bedside and in emergency medicine [1]. Typical US imaging employs a pulse-echo approach that involves transmitting an acoustic signal into the tissue and receiving the fraction of the signal that is returned as echoes. The backscattering intensity depends on the acoustic impedance (Z) mismatches at the various interfaces or between the scatterers within the tissue. Broadly, the interfaces/scatterers are either diffuse or specular according to their relative sizes with the wavelength of the US signal. The reflections/scattering are diffuse if the dimension of the reflecting surface is very small compared to the US wavelength [2]. The small sizes of scatterers cause the US to be backscattered in multiple directions reducing the reflected intensity. However, if the surface thickness is very large relative to the wavelength, the reflections are specular. Such reflections follow Snell's law (mirror-like reflections) and have high intensity and directivity that depends on the reflector orientation and the angle of incidence of the US signal on the interface [2], [3].

The lung parenchyma is composed of both diffuse and specular interfaces. In a healthy condition, it is a judicious combination of air, fluid, and tissue surrounded by a thin membrane pleura [4]. The large Z mismatch between the air-pleura interface and high attenuation of US in air restricts its penetration through the lung to further depths. In this regard, the artifacts resulting from the above peculiar physical characteristics of the lung are used for anatomic interpretation to distinguish between the different lung conditions. In a normal lung, due to the large Z mismatch between the air and the pleura, the interface acts as a strong specular reflector causing multiple reverberations between the interface and the transducer. The reverberations appear as artifacts, which are hyperechoic lines of decreasing intensity with depth, parallel and beneath the pleura at equidistant intervals, and are called A-lines [1], [4]. However, in a pathologic lung, the specularity of the air-pleura interface is altered due to the reduced air content and increased density in the sub-pleural space due to the presence of fluid, or edematous tissue. Consequently, the Z mismatches are lowered and the lung parenchyma tends towards the diffuse regime [4], [5]. The presented work focuses on two such pulmonary conditions. One is the interlobular septal thickening (IST) due to fluid accumulation. The thickened septa surrounded by air act as channels for the US to penetrate larger depths resulting in the appearance of discrete hyperechoic artifacts called B-lines. They originate from or below the pleural line, extend to the bottom, obliterating the A-lines, and their frequency of appearance directly correlates to the severity of edema [4], [6], [7]. Another is a more critical pulmonary condition, which is sub-pleural consolidation due to the filling of air sacs with fluid, pus, or blood. This is characterized by the presence of nodulations, and irregular and thickened pleura [4].

However, understanding the normal and abnormal pulmonary conditions through characterizing the reflections as specular or diffuse from and around the air-pleura interface has not been investigated in detail in the literature. This may be due to the difficulty in obtaining real-time radio-frequency (RF) data of the normal and pathological lung. Though multiple experimental lung models/phantoms have been proposed [6], [7], [8], the experimental setups, their

*Research supported by Department of Science and Technology - Science and Engineering Research Board (CVD/2020/000221) and the Ministry of Education, India.

Gayathri Malamal and Mahesh Raveendranatha Panicker are with the Center for Computational Imaging, Indian Institute of Technology, Palakkad, India (e-mail: 121814001@smail.iitpkd.ac.in; mahesh@iitpkd.ac.in).

repeatability, could be difficult and expensive for research labs with limited resources. Therefore, it is detrimental to have equivalent simulation models that could supplement and complement the experimental models and also provide a better insight to clinicians into the physics of lung behavior. To the best of our knowledge, simulation models replicating the different lung conditions are hardly found in the literature.

In this work, we propose three simulation models for the lung using k-Wave US toolbox [9] representing the normal (A-lines), edematous (B-lines), and sub-pleural consolidation states (i.e., the increasing order of severity) [4]. Further, we propose a novel approach of characterizing reflections by deriving a pixel intensity vector field (PIVF) that maps the acoustic intensity from each pixel in the scan plane to the transducer plane for each lung model. Though in this work, PIVF approach is directed to the lung, it is equally applicable to any tissue and is a boost to the pixel-level beamforming that is proposed in our previous work [10].

II. Methods

A. Modeling of pulmonary conditions

In this work, three models representing normal, edematous, and consolidated lung are simulated with k-Wave US toolbox [9]. The toolbox inputs the transducer model, the speed of sound (SoS) (m/s), density (kg/m^3), and attenuation (dB/(cm-MHz)) maps of the models to mimic the physical US acquisition setup. In our simulations, the transducer is modeled based on the physical L11-5v linear array transducer [11] used with the Verasonics Vantage 128 channel (Kirkland, USA) US research platform in our lab. It is a 1-D probe with a bandwidth of 4.2–10 MHz Commonly, pleural ultrasonography is performed with linear probes of frequencies between 3.5–5 MHz [12]. Considering this and aligning with the specifications of the L11-5v transducer [11], the transmit center frequency is set to 4.8 MHz. The SoS, density, and attenuation maps are modeled with values provided in [13]. As k-Wave is unable to handle sudden changes in density, the density of air is taken as 100 kg/m^3 against the standard to ensure simulation stability. A grid size of 4.1 cm x 4.1 cm or 1200 x 1200 grid points with a grid spacing of $\lambda/2$ where, λ is the wavelength of the medium with the least SoS (in this case, air) including a perfectly matched layer (PML) of 20 grid points as suggested by the toolbox is chosen for ensuring a stable simulation. A random scatterer distribution is included to create heterogeneity in the tissue. The Courant-Friedrichs-Lewy (CFL) number is chosen as 0.05. The models are simulated assuming that the probe is positioned along the mid-clavicular line (longitudinally and perpendicular to the ribs) [5].

The first model is a normal lung (NL), which visualizes soft tissue above the pleura, the pleural line in the intercostal space, and the sub-pleural space which is fully aerated. The thickness of the normal pleura is 0.2-0.4mm [12]. In the model, a thickness of 0.3mm is chosen with the values of SoS, density, and attenuation as that of the soft tissue as illustrated in Fig. 1. The second model simulates an edematous lung (EL) where the interlobular septa that connect to the pleura are thickened due to fluid accumulation. The IST is achieved by introducing a triplet of layered fluid bubbles of a radius of 1440 µm to create acoustic channels for penetration of US within the aerated lung [6]. The SoS, density, and attenuation maps are

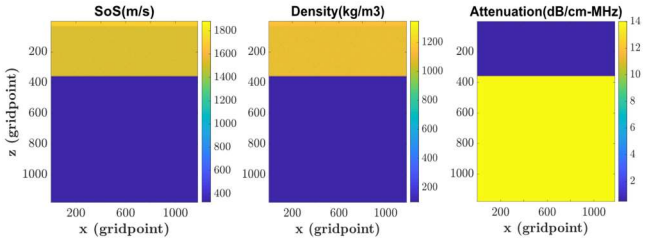

Figure 1: SoS, density and attenuation maps for normal lung

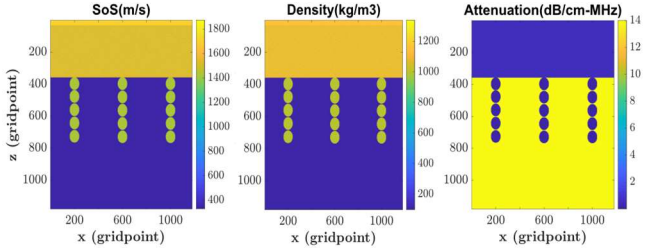

Figure 2: SoS, density and attenuation maps for edematous lung.

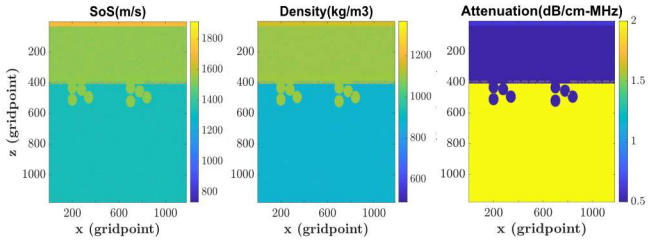

Figure 3: SoS, density and attenuation maps for consolidated lung.

presented in Fig. 2. The third model is a consolidated lung (CL) which is simulated here as a case of pleural inflammation (thickening), effusion, and presence of nodulations below the pleura [6], [14]. The pleural surface is scarred and invades into the air spaces forcing the lung into a deaerated state as the air spaces get isolated. The sub-pleural region becomes denser and tends towards the soft tissue. Fig. 3 shows the SoS, density, and attenuation maps of the simulated model.

A. Pixel Intensity Vector Field (PIVF)

It is already discussed that the altering of the air-pleura interface is an indication of the severity of the lung pathology and it manifests as a shift from specular reflections to diffuse scattering. In this section, we propose a novel approach to characterize the tissue reflections through estimating the pixel intensity vector field (PIVF). Consider a scan plane S of N_P pixels, which are insonated by plane wave (PW) transmissions using a linear array transducer of N_c elements. The PW transmissions enable high frame rate imaging. For a pixel k in S, the received intensity on each channel at any instant of time is a function of the distance from the pixel to the channel, the distance from transmit center to the pixel, and the type of scatterer/reflector. The final beamformed signal of the k^{th} pixel, y_k is obtained by the summation of the signals received at each channel after delay compensation for each PW transmit angle (delay and sum (DAS)) [15], [16], as in (1).

$$y_k = \sum_{j=1}^{M} \sum_{i=1}^{N_c} W_{i,k}\, x_{i,j}(\tau_{i,j}(k)) \qquad (1)$$

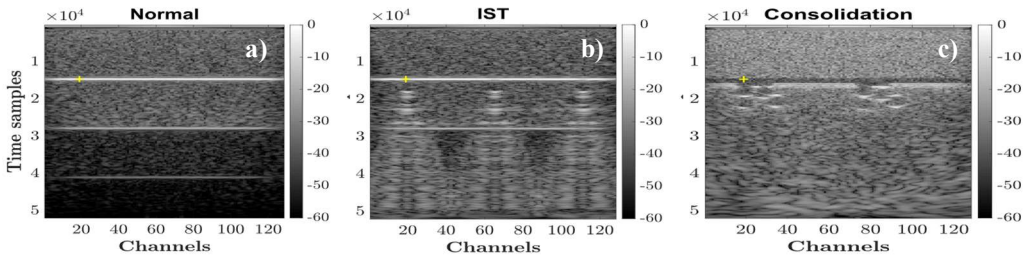

Figure 4: Beamformed images for a) Normal b) Edematous c) Consolidated lung models

where, M is the total number of transmitted PWs with inclination angles $\alpha_T = [\alpha_1, \alpha_2, \ldots, \alpha_M]$, $W_{i,k}$ is the apodization weight of the i^{th} element, $x_{i,j}(\tau_{i,j}(k))$ is the time-aligned signal after compensating with the two-way delay $\tau_{i,j}$ as in [15], [16]. The delay compensation makes up for the mismatch in the arrival time of the signals in each channel due to the varied distance from the pixel k. The apodization enhances the reflections from the pixel by proportionally weighing each channel according to the geometric distance from the pixel assuming it is diffuse. However, this may suppress the directive specular reflections that violate the geometric distance rule due to the reflector orientation or angle of incidence of the transmitted PW [3]. The final summed signal y_k, therefore, may not be an accurate estimate of the reflected intensity.

In the proposed approach, (1) is dissected from the perspective of a vector field in a 2-D space. The insight is that acoustic intensity from each pixel is a vector with a magnitude and, direction depending on the nature of the pixel (diffuse/specular). It results in an intensity vector field V that is a projection of the acoustic intensity of each pixel k in S to the transducer plane T consisting of N_c elements. Mathematically, the vector field could be represented as in (3) where S and T are subsets of R^2.

$$V := S(k) \rightarrow T \tag{3}$$

For each $\alpha_j \in \alpha_T$, where $j = [1, M]$, the magnitude of each vector in V provides the strength of the reflected intensity and the direction gives the distribution of reflected intensity from the pixel to the corresponding transducer element. This directly associates with the scatterer characterization because if the scatterer is diffuse, V tends to be a uniform field. While, if the pixel belongs to a specular region, V is non-uniform and the field dominates in the direction of maximum reflection which is governed by PW transmit angle and reflector orientation [3].

III. Results and Discussion

The three k-Wave lung models are simulated in MATLAB R2019a employing high frame coherently compounded PW imaging [16]. The PWs are transmitted at α_T = [-10º, 0º, 10º]. The RF data obtained from the models are time gain compensated assuming a homogenous attenuation value of 0.5 dB/(cm-MHz). Further, they are beamformed as in (1), envelope extracted, and log compressed to display in an interpretable format. The beamformed image of the NL is shown in Fig. 4 a). Observations from Fig. 4 a) prove the specularity of the air-pleura interface with the appearance of horizontal hyperechoic A-line reverberation artifacts at equidistant intervals below the pleura. The A-lines deteriorate with depth due to intensity degradation with each reverberation between the transducer and air-pleura interface. Fig. 4 b) shows the beamformed image of the EL model. The acoustic channels of fluid that are created due to IST and are surrounded by air act as a source of acoustic vibrations. This results in vertical artifacts called B-lines that originate from below the pleura and reaches down to the bottom depending on the amount of energy that has permeated through the fluid channels, attenuation in the fluid medium, and the amount of energy returning to the transducer [6]. The specularity of the air-pleural interface has deteriorated and has completely faded off the second and partially the first A-lines that existed in Fig. 4 a). The presence of more acoustic channels in the sub-pleural space will further reduce the air content in the lung causing respiratory distress. This is evident in the beamformed image of the third model illustrating a CL that is shown in Fig. 4 c). The pleura has thickened and become irregular. The anechoic

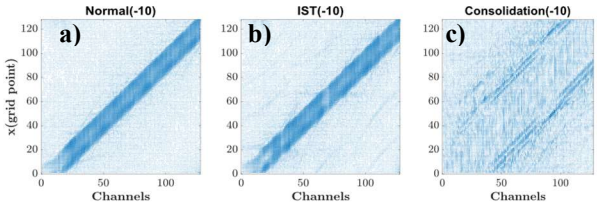

Figure 5: PIVF along air-pleura interface for PW transmission with $\alpha_T = -10°$ for a) Normal b) Edematous c) Consolidated lung

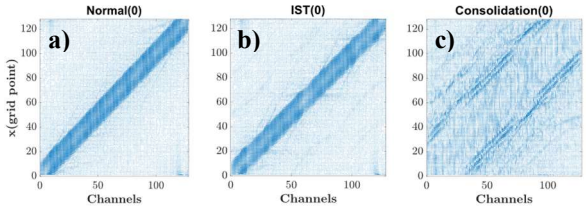

Figure 6: PIVF along air-pleura interface for PW transmission with $\alpha_T = 0°$ for a) Normal b) Edematous c) Consolidated lung

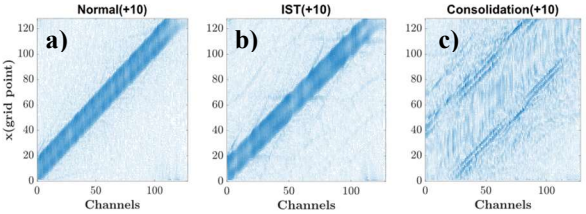

Figure 7: PIVF along air-pleura interface for PW transmission with $\alpha_T = +10°$ for a) Normal b) Edematous c) Consolidated lung

region of the pleural space indicates effusion and there is an appearance of small consolidated regions below the pleura extending to the air spaces. The sub-pleural region has become denser creating more pathways for US penetration. Assuming

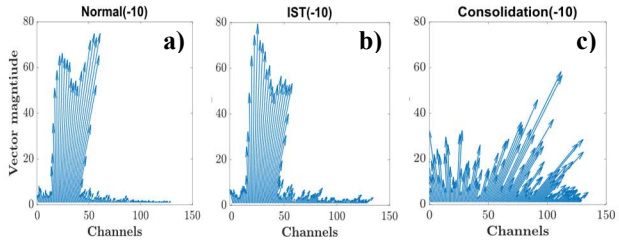

Figure 8: PIVF for PW transmission with $\alpha_T = -10°$ for a) Normal b) Edematous c) Consolidated lung

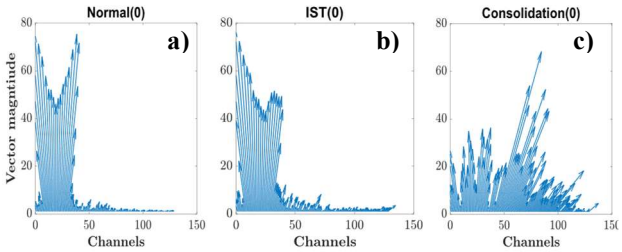

Figure 9: PIVF for PW transmission with $\alpha_T = 0°$ for a) Normal b) Edematous c) Consolidated lung

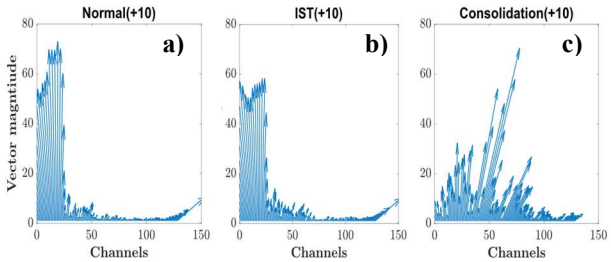

Figure 10: PIVF for PW transmission with $\alpha_T = +10°$ for a) Normal b) Edematous c) Consolidated lung

the air-pleura interface to be without tilt, and considering the directive specular reflections in the NL and EL models, a Tukey window receive apodization with a roll of factor 0.25 and F-number = 1.5 is employed during beamforming. For the CL, F-number = 0.5 is chosen to accommodate the diffuse scattering.

Further, the PIVF along the air-pleura interface (at a depth indicated by yellow '+' in Fig. 4) is plotted for all α_Ts. The results are presented in Fig. 5 - Fig. 7. It is seen that as we move from NL to CL, the spatial distribution of acoustic field lines is altered from a denser to a scattered distribution. This is more evident from Fig. 8 - Fig. 10 in which a scaled PIVF plot for a single pixel alone (pixel indicated in yellow '+' in Fig. 4) is plotted. In NL and EL models, there is a presence of a dominant directive acoustic field. But in EL, the field lines are a little staggered relative to NL indicating the onset of shifting to diffuse domain. However, in CL, specularity is completely lost resulting in a scattered vector field. It should be also noted from the slight tilting of dominant directions (~ channels 1-50) in the vector field plots of NL and EL that there is an influence of PW transmit angles (Snell's law of reflection [3]) whereas the vector field direction in the CL model is less dependent on the same.

It could be concluded that the proposed PIVF approach gives a good qualitative characterization of the US reflections from the lung. This also point towards the need of a non-diffuse beamforming for lung US. A detailed analysis of the approach combined with quantitative characterization concerning different tissues will be dealt with as future work.

APPENDIX

The video demos illustrating the acoustic pressure distribution for all three simulation models (with grid sizes and parameters scaled for better visual perception) are available in the link shorturl.at/kswD9.

ACKNOWLEDGMENT

The authors would like to acknowledge funding from the Department of Science and Technology - Science and Engineering Research Board (CVD/2020/000221) and the Ministry of Education, India.

REFERENCES

[1] D. A. Lichtenstein, "Lung ultrasound in the critically ill," *Ann. Intensive Care*, vol. 4, p.1, 2014.

[2] T. Szabo, Diagnostic Ultrasound Imaging, 2nd ed. Academic Press, 2014.

[3] A. Rodriguez-Molares, A. Fatemi, L. Løvstakken, and H. Torp, "Specular Beamforming," *IEEE Trans. Ultrason., Ferroelectr., Freq. Control*, vol. 64, no. 9, pp. 1285-1297, 2017.

[4] G. Soldati G, M. Demi, R. Inchingolo, A. Smargiassi, and L. Demi, "On the Physical Basis of Pulmonary Sonographic Interstitial Syndrome", *J. Ultrasound Med*, vol. 35, no. 10, pp. 2075-2086, 2016.

[5] G. Luna and G. Volpicelli, "How I do it: Lung ultrasound", *Cardiovascular ultrasound*, vol. 12, no. 25, 2014.

[6] M. Demi, R. Prediletto, G. Soldati, and L. Demi, "Physical Mechanisms Providing Clinical Information From Ultrasound Lung Images: Hypotheses and Early Confirmations," *IEEE Trans. Ultrason., Ferroelectr., Freq. Control*, vol. 67, no. 3, pp. 612-623, 2020.

[7] Soldati G, Giunta V, Sher S, Melosi F, Dini C: ""Synthetic" comets: a new look at lung sonography", *Ultrasound Med. Biol.*, vol. 37, pp. 1762-1770, 2011.

[8] C. Blüthgen, S. Sanabria, T. Frauenfelder, V. Klingmüller, and M. Rominger, "Economical sponge phantom for teaching, understanding, and researching A- and B-line reverberation artifacts in lung ultrasound," *J. Ultrasound. Med*., vol. 36, no. 10, pp. 2133–2142, 2017.

[9] B. Treeby and B. Cox, "k-Wave: MATLAB toolbox for the simulation and reconstruction of photoacoustic wave fields," *J. Biomed. Opt.*, vol.15, pp. 021314, 2010.

[10] G. Malamal and M. R. Panicker, "Towards A Pixel-Level Reconfigurable Digital Beamforming Core for Ultrasound Imaging," *IEEE Trans. Biomed. Circuits Syst.* , vol. 14, no. 3, pp. 570-582, 2020.

[11] Verasonics transducer specifications, 2017 [Online]. Available: https://verasonics.com/wp-content/uploads/2017/11/Transducer_specifications_sheet_2017.pdf

[12] Mayo PH, and Doelken P, "Pleural ultrasonography", *Clin. Chest Med,* vol. 27, pp. 215-227, 2006.

[13] H. Stephen, Medical ultrasound imaging, Physics Education, 36. 468, 2001. 10.1088/0031-9120/36/6/304.

[14] F. Dietrich, G. Mathis, X.-W. Cui, A. Ignee, M. Hocke, and T. O. Hirche, "Ultrasound of the pleurae and lungs," *Ultrasound Med. Biol.*, vol. 41, no. 2, pp. 351–365, 2015.

[15] Vincent Perrot, Maxime Polichetti, François Varray, and Damien Garcia, "So you think you can DAS? A viewpoint on delay-and-sum beamforming", *Ultras.*, vol. 111, 2021.

[16] G. Montaldo, M. Tanter, J. Bercoff, N. Benech, and M. Fink, "Coherent plane-wave compounding for very high frame rate ultrasonography and transient elastography," in *IEEE Trans. Ultrason., Ferroelectr., Freq. Control*, vol. 56, no. 3, pp. 489-506, 2009.